Geoelectrical imaging in the interpretation of geological conditions affecting quarry operations

Magnusson, Mimmi K.; Fernlund, Joanne M. R.; Dahlin, Torleif

Published in:
Bulletin of Engineering Geology and the Environment

DOI:
10.1007/s10064-010-0286-y

2010

Bull Eng Geol Environ (2010) 69:465–486
DOI 10.1007/s10064-010-0286-y

ORIGINAL PAPER

Geoelectrical imaging in the interpretation of geological conditions affecting quarry operations

Mimmi K. Magnusson · Joanne M. R. Fernlund · Torleif Dahlin

Received: 10 May 2009 / Accepted: 18 March 2010 / Published online: 6 July 2010

Abstract Determination of the subsurface geology is very important for the rock quarry industry. This is primarily done by drilling and mapping. However, in Sweden, the bedrock is often completely covered by Quaternary sediments, making the prediction quite difficult. This study shows that electrical resistivity imaging together with induced polarization proved to be very efficient in detecting fracture frequency, major fracture zones and variations in rock mass quality, all of which can affect the aggregate quality. These techniques can also determine the thickness of the overburden. Furthermore, by doing 2D-parallel data sampling, a 3D inversion of the dataset is possible, which greatly enhances the visualization of the subsurface. Implementation of geophysics can be a valuable tool for the quarry industry, resulting in substantial economic benefits.

Keywords Electrical resistivity imaging · Rock mass quality · Aggregate production · Geophysical methods · Induced polarization · Normalized induced polarization

Résumé Les études géologiques de sub-surface sont très importantes pour l'industrie des matériaux de carrière. Ces études sont principalement réalisées par forage et cartographie. Cependant, en Suède, le substratum est souvent complètement recouvert par des dépôts quaternaires, entraînant des prévisions très difficiles. Cette étude montre que les techniques associées d'imagerie de résistivité électrique et de polarisation induite s'avèrent être très efficaces pour la détection de densités de fractures, de zones fortement fracturées et de variations de la qualité du massif rocheux, tous ces éléments pouvant affecter la qualité des granulats. De plus, en réalisant des échantillonnages par des lignes parallèles à deux dimensions, une inversion tridimensionnelle du jeu de données est possible, ce qui améliore grandement la visualisation de la sub-surface. La mise en œuvre des méthodes géophysiques apparaît intéressante pour les industries extractives, avec en perspective des bénéfices économiques substantiels.

Mots clés Imagerie de résistivité électrique · Qualité de massif rocheux · Production de granulats · Méthodes géophysiques · Polarisation induite · Polarisation induite normalisée

M. K. Magnusson (✉) · J. M. R. Fernlund
Department of Land and Water Resources Engineering, Royal Institute of Technology (KTH), Teknikringen 72, 100 44 Stockholm, Sweden
e-mail: mimmia@kth.se

T. Dahlin
Department of Engineering Geology, Lund University, Box 118, 221 00 Lund, Sweden

Introduction

Aggregates (crushed rock fragments) are used for many different purposes, e.g. railway construction, roads and concrete. To date, Sweden has produced most of its aggregate from sand and gravel pits from natural sources, such as eskers and other glaciofluvial deposits. However, eskers are very important for groundwater extraction and the purification of lake water. Environmental goals for sustainable building require increased preservation of eskers and thus the government aims to decrease the use of natural sand and gravel and increase the use of recycled aggregate material. As a result, it is very hard to get new permits for the production of aggregates from natural

gravel sources. Instead aggregates are produced from rock quarries as well as from the recycling of asphalt and concrete, and from other alternative materials.

Rock quarries are often associated with a negative environmental impact, such as noise and air pollution, and it can therefore be difficult to obtain public support for establishing a new rock quarry. If a rock quarry is to be established, it is important that the rock mass is suitable for aggregate production. It is not easy to know the properties of the rock mass in Sweden, which is predominantly composed of Precambrian crystalline rocks that have undergone numerous tectonic events. In some areas, the rock mass is relatively homogeneous whereas in other areas the mass consists of many different rock types, sometimes occurring in thin bands, all with different mechanical properties. Uniform rock mass quality is important in order to ensure uniform aggregate quality.

The rock mass in Sweden is covered to a large extent by glacial deposits, but drill holes only give information of the rock at the drill sites and interpreting potential homogeneity or variations in the rock mass quality from a few drill cores is risky. Furthermore, drilling is very expensive and it is difficult to determine variations in the rock mass composition as well as the existence of weathered zones or dykes, joint/fracture frequency and orientation, thickness of overburden, water-bearing zones or weak rock prone to sliding. The interpretation of the rock mass quality from drill holes is therefore complemented by a study of outcropping rock bodies. The risk, however, is that these are the more resistant/stronger horizons.

Prior to quarrying, it is important to determine variations in composition of the rock mass (Räisänen and Torppa 2005) such that undesirable rocks are avoided, variable rock types can be blended to maintain a more uniform quality and the direction of quarrying can be controlled in order to ensure safer rock faces and good fragmentation from blasting. In addition, the overburden thickness affects the viability of quarrying the aggregate.

Geophysical measurements potentially can be a useful tool for quarry prospecting and for optimization of quarry expansion. The electrical resistivity technique is a well-established method, which can be applied to a wide range of hydrogeological, geological, engineering and environmental problems (Bowling et al. 2007; Sass 2007; Drahor et al. 2006; Aaltonen and Olofsson 2002; Dahlin 2001; Atekwana et al. 2000). Electrical resistivity can identify variations in the type of rock mass, joint spacing and orientation as well as the composition and thickness of the overburden. However, the use of geophysical measurements within the rock quarry industry is generally fairly limited.

Electrical resistivity imaging (ERI) can yield a continuous picture of the subsurface conditions. In order to ensure a correct interpretation of the geophysical study, check drilling is needed, but the profiles can be used to make more efficient choices for the location of the drill holes (Dahlin 1997). Opening rock quarries in a rock mass that will produce good quality aggregates and less waste material as well as maximizing the production of good quality material can lead to a substantial economic saving for the aggregate industry plus an environmental saving for society.

The aim of this paper is to show how geoelectrical imaging can be used to predict rock and overburden characteristics prior to opening a rock quarry and to optimize the expansion of quarries, primarily with respect to (1) detection of quality variation in the rock mass, (2) orientation of joints and fractures and other discontinuities, and (3) thickness and composition of the overburden.

Description of sites

The Precambrian crystalline rocks in Sweden are overlain unconformably by Quaternary unconsolidated sediments, mostly till. Three rock quarries in a similar rock mass but with variable fracture frequency (low, medium, high) were chosen for this study. The Olunda site is situated north of Stockholm, the Bäckseda site is situated south of Vetlanda in southern Sweden, and the Dalby site is situated north of Malmö in the southernmost part of Sweden (Fig. 1). The till at the sites is assumed to be from the Late Weichselian glaciation.

Olunda

The Olunda site is located at about 35–40 m above present sea level, well below the highest postglacial shoreline, which is about 150 m asl in this region. The topography is slightly undulating, varying by up to 10 m in altitude over 2 km^2. The bedrock at Olunda is composed of granodiorite to tonalite (Arnbom and Persson 2001) with widely spaced (>1 m) healed, tight joints (Fig. 2). In a few places, the fracture frequency is higher. The bedrock in the map sheet area (25 km^2) is composed predominately of granite and granodiorite. North of the site, there are a couple of areas (>4 km^2) of metavolcanics as well as a few small bodies (<1 km^2) of metamafic, gabbro to diorite rocks.

The bedrock is overlain by glacial till, which in turn is overlain in part by glacial and postglacial clay and other postglacial sediments. The till is mainly sand and silt with a number of predominantly angular boulders (ca. 2 m^3), as is common in this area (Möller 1992, 1993). The till seldom exceeds 4 m thickness in the region; the glacial striations indicating a variation of ice flow directions (Möller and Stålhös 1971, 1974).

Fig. 1 Location of the study areas

Fig. 2 *Top* quarry face at Olunda, *bottom* surface at Olunda after removal of the overburden

Bäckseda

The Bäckseda site is located on top of a hill at about 280 m asl. The general relief varies up to 100 m vertically within 2 km^2 but in the study area, the amplitude is <8 m. It is above the postglacial sea level, which here is >100 m asl.

The bedrock at Bäckseda is granite with regular fractures at spacings of <200 mm (Fig. 3). The bedrock in the map sheet area (Persson 1988, 1989) is much more diverse than at Olunda, with some 60% felsic rocks (granite, granodiorite, tonalite, quartzdiorite, and pegmatite) and 30% metasediments and metavolcanics. There are a few occurrences of mafic rocks (diabase dykes) and porphyritic metavolcanics, porphyritic granite, granite porphyry, and porphyritic dykes.

Some 72% of the surface is covered by a predominantly sand and silt till. A few boulders are present, normally subrounded and <50 cm^3 in size.

Dalby

The Dalby site is located approximately 70 m asl, on the Romelåsen horst, which trends NW–SE. The surface is relatively flat, varying at most by 5 m. The site is above the

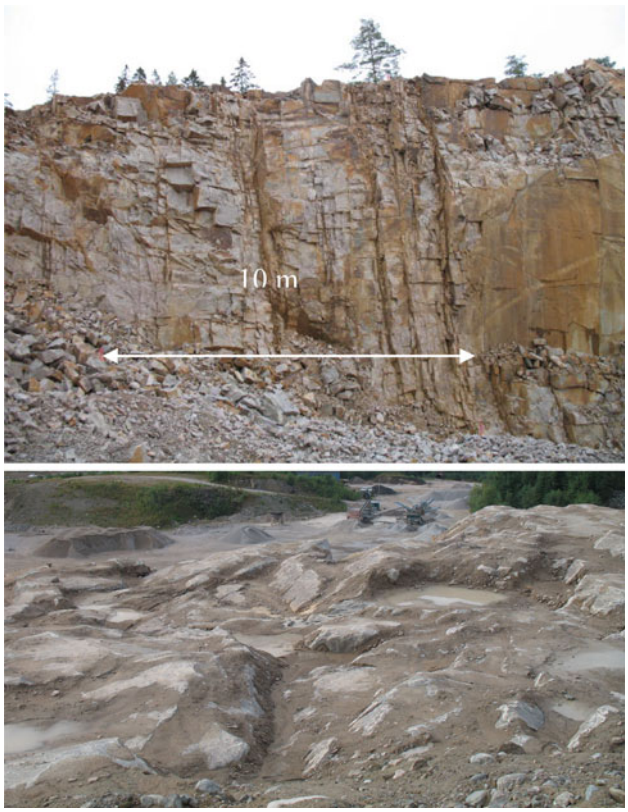

Fig. 3 *Top* quarry face at Bäckseda, *bottom* surface at Bäckseda after removal of the overburden

postglacial shoreline which, although controversial, is clearly below 50 m in this area (Ringberg 1980). The bedrock of the horst consists mainly of Precambrian metamorphosed red aplite (Sivhed and Erlström 1998) referred to in the industry as gneissic aplite, with the gneissic foliation trending N–S. It is highly jointed (Fig. 4) with a number of inclusions of metavolcanics and four different types of dykes (Ringberg 1979).

The first type of dykes consists of basic rocks, which were metamorphosed at the same time as the aplite and changed to amphibolite. The second group is composed of hyperite, porphyry, and porphyrite with an orientation similar to the foliation of the aplite. The third group also consists of hyperite dykes that are oriented NNE to SWW and up to a metre in thickness. These dip steeply to the west. The fourth group consists of diabase, probably formed some 290 million years ago (Bylund 1973; Klingspor 1976) and prior to the formation of the horst (Müllern 1978). They vary in trend, NW–SE and WNW–ESE.

The Quaternary deposits in the region of Skåne are very different from the rest of Sweden, probably due to the sedimentary nature of the bedrock. The ice flow direction has varied extensively, with evidence of ice flow from the north as well as from the south. The Quaternary sediments are exceptionally thick in Skåne, over 120 m in some places. However, the thickness of the till overlying the horst seldom exceeds 5 m, except in localized depressions/pockets. There are at least five different tills in the area, the most common having a clay content between 5 and 10% and a predominantly silt and sand matrix. The high cobble content consists mainly of Precambrian clasts with a few boulders. A second, almost boulder-free deposit is also present and an inter-till sand and gravel sediment has also been identified as well as postglacial aeolian/fluvial sand in depressions and valleys.

Fig. 4 *Top* quarry face at Dalby, note the diabase dyke in the middle, *bottom* surface at Dalby, after removal of the overburden

Methods

The two geophysical methods used for this study were ERI and induced polarization (IP).

Electrical resistivity imaging

The electrical resistivity instrument is connected to electrodes, using separate electrodes for current transmission and potential measurement (Fig. 5). The electrodes are inserted a few decimetres into the ground, in a straight line with equal spacings between the electrodes. A current is passed into the ground and the voltage between the potential electrodes measured simultaneously. The potential measured depends on the resistivity distribution of the subsurface material. A geometrical factor must be used to calculate the resistivity of the ground (Ωm) from the measured resistance (Ω), which is specific for the chosen electrode geometry. The measured resistivity depends on the nature of the investigated earth volume, which would only be equal to the true resistivity in a homogeneous material; hence the measured value is referred to as apparent resistivity. In order to estimate the true resistivity distribution of the ground, it is necessary to generate a model of the ground, which is adjusted so that the model fits a set of measured data; this is generally done using inverse numerical modeling (inversion).

The resistivity values of different geological materials vary considerably (Fig. 6). For till, the values typically range from just a few Ωm to several thousand Ωm, while for granite, the range is typically from a few hundred to 10^6 Ωm (Palacky 1989). In most soil and rock types, the mineral grains are isolators and the resistivity is governed by the water content and ions in the pore water and within the mineral grains. As the amount of water and ions in the water increases in the material, the resistivity of the material decreases. The clay content is also an important factor because clay minerals are themselves electrically charged and are in electrical equilibrium with the adjacent pore water (Zonge et al. 2005; Palacky 1989); thus, the greater the clay content (notably in weathered rocks), the

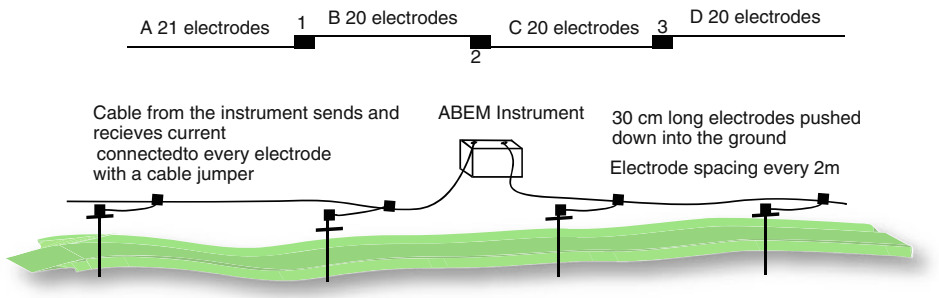

Fig. 5 Instrument set-up for ERI and IP

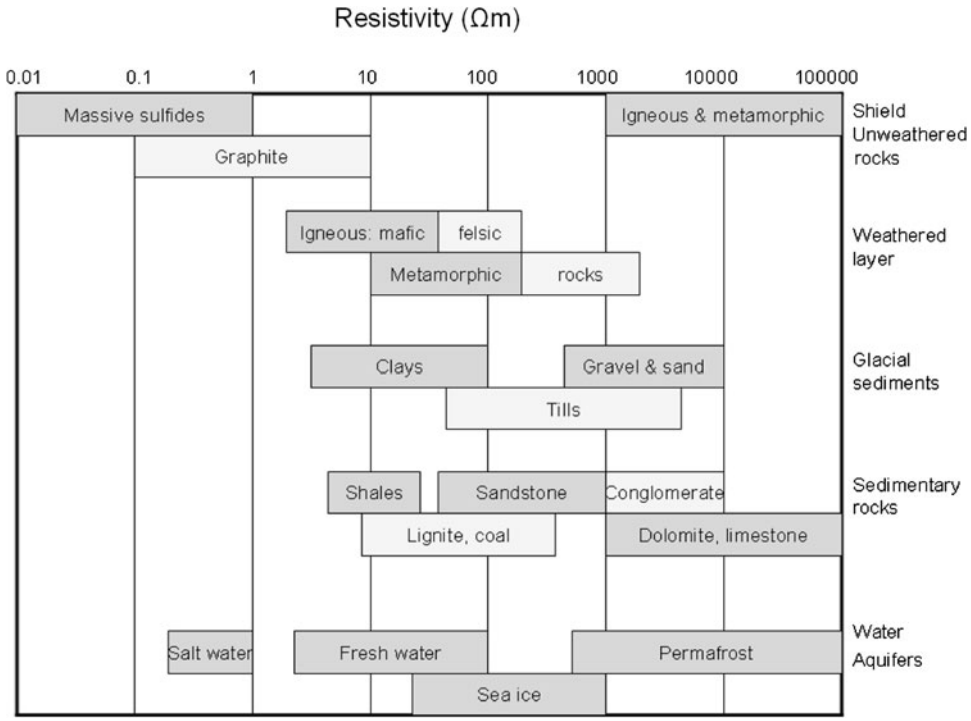

Fig. 6 Typical ranges of resistivities of earth materials, modified from Palacky (1989)

lower the resistivity. Massive sulphides and graphite are very conductive and have resistivity values below 10 Ωm (Fig. 6). Graphite is often the connecting link in mineral zones (Telford et al. 1990).

Fresh, fracture-free crystalline rock has a very low (almost non-existent) water content, resulting in high resistivity values. Highly fractured and highly weathered rock normally contains a substantial amount of water in cracks and pores, which together with the mineralization which often occurs in the fractures, results in low resistivity values. As a consequence, it is possible to interpret variations in rock quality, with respect to fracture frequency and weathering, from the resistivity values.

The resistivity of the unconsolidated sediment depends on its composition and water content, which is related to permeability and capillarity. Cohesive soils have adsorbed layers and high capillarity thus very low resistivity values (Fig. 6). Non-cohesive (sand and coarser-grained) material is highly permeable and its resistivity will depend on its position with respect to the groundwater table.

For poorly sorted/well-graded soils, such as till, the resistivity depends on several factors. Poorly sorted material generally has a low pore volume and low water content and hence would be expected to have a higher resistivity. However, the proportion of cohesive material when compared with the larger rock fragments is equally important; the higher the percentage of cohesive material the lower the resistivity. As a consequence, due to the heterogeneous composition of tills, the resistivity can vary substantially, although it is usually within 50–2,000 Ωm (Palacky 1989). Without geological reference data, a higher resistivity of the till (compared to the bedrock) might lead to wrong conclusions about the thickness of the till.

Normally, the groundwater level in the unconsolidated sediment overlying crystalline rocks in Sweden is between 1 and 2 m below the ground surface. However, due to

pumping, the groundwater level is lowered in the vicinity of the quarry, resulting in abnormally high resistivities (Wisén et al. 2006). This also needs to be borne in mind when interpreting the data.

Induced polarization

In this method, the current is first sent into the ground, the total observed potential, V, is measured and then the current is turned off. After a short time (e.g. 0.01 s), the potential which is still in the ground is measured at discrete intervals of time, typically 0.1 s. The readings can be combined to yield a current decay curve. The measured IP is often expressed as chargeability (mV/V).

The IP is a function of lithology and the fluid conductivity of the rocks/soils. Sources that can give an IP response are layered silicates, clays, metallic lustre minerals, organic materials and anoxic carbon-rich deposits, and other iron-rich minerals such as limenite and hematite (Zonge et al. 2005). The surface area of the metallic grains is also important for the response of the IP, which increases with increased surface area.

Slater and Lesmes (2002) reported that chargeability is strongly correlated with resistivity and suggested dividing the IP result by the resistivity to give a normalized IP (NIP) with the unit in Siemens, mS/m. They showed that NIP is proportional to the conductivity. This method highlights areas with different surface conductance properties, while removing the conductance caused by the fluid in the pore spaces.

Data acquisition using the IP method is more complicated as it involves small measured voltages and short integration times. With some electrical resistivity equipment, it is possible to measure IP at the same time as ERI, to complement it. This is particularly useful where noise affects the IP data as the ERI data will almost always be acceptable (Dahlin et al. 2002; Leroux and Dahlin 2003; Maia and Castilho 2008). Electrode contact resistance also plays an important role, and generally high resistivity material at the surface is problematic.

Field studies

The field studies comprised ERI and IP measurements, determination of the thickness and composition of the overburden and determination of the fracture frequency of the rock mass. At each site, the area studied was a grid approximately 50 m from the active quarry face (Figs. 7–9), hence the interpretations of the data will eventually be verifiable as the quarry expands. The length of the grid was 160 m, to allow for four 40 m cables for the geophysical measurements (Fig. 5) and there were 11 lines at 4 m spacings. The topography of the ground surface was determined using a theodolite and the corners of the grid located using GPS; it was not possible to measure the entire three grids with GPS as the areas were partly forested.

Both the orientation and the starting point of the assigned coordinates of the grids varied at the three sites.

In Olunda (Fig. 7), the long axis of the grid was oriented E–W and the short axis N–S. The starting point for the coordinate system, $x = 0$, $y = 0$ was in the NE corner of the grid. Note that this was at Line 2, as the data from Line 1 was faulty. The positions in the results are referenced as coordinates x, y, z.

In Bäckseda (Fig. 8), the long axis of the grid was oriented E–W and the short axis N–S. The starting point of the coordinate system, $x = 0$, $y = 0$ was in the SW corner of the grid.

In Dalby (Fig. 9), the long axis of the grid trends N310° and the short axis N040°. The starting point of the coordinate system, $x = 0$, $y = 0$, was in the corner located furthest to the south.

ERI and IP field measurements

The ERI instrument used was slightly different at each of the three sites; three different versions of the ABEM Lund Imaging System. All the instruments allow time efficient multi-channel data acquisition, and in all cases the multiple-gradient electrode configuration was used. This provides very stable field-data acquisition, with a good signal-to-noise ratio (Dahlin and Zhou 2006).

The data were collected as 2D resistivity imaging sections along each of the grid lines with a 2 m interval between the electrodes (Fig. 5). The instrument is first placed at position one and connected to the three first cables for its first measurement, then the instrument is moved to the second position and connected to all four cables. For the third and last position, the instrument is connected to the three last cables, thus cable one is not used. The 4 m spacing between the lines is double the electrode distance, the required distance for good subsurface results (Gharibi and Bentley 2005). The acquisition strategy of combining 2D sections can be considered to be a roll-along procedure for 3D surveying. This measuring strategy allowed a 3D inversion of the data, which gives increased detail and accuracy of the resulting resistivity model when compared with 2D inversion (Dahlin et al. 2007; Papadopoulos et al. 2007).

The instruments used can also measure IP, although at Olunda the IP was not measured due to limitations in the firmware in the instrument. It was also necessary to water the electrodes at Olunda, to increase the contact between the electrodes and the overburden due to the dry conditions when the fieldwork was being performed. This was not necessary for the other two sites.

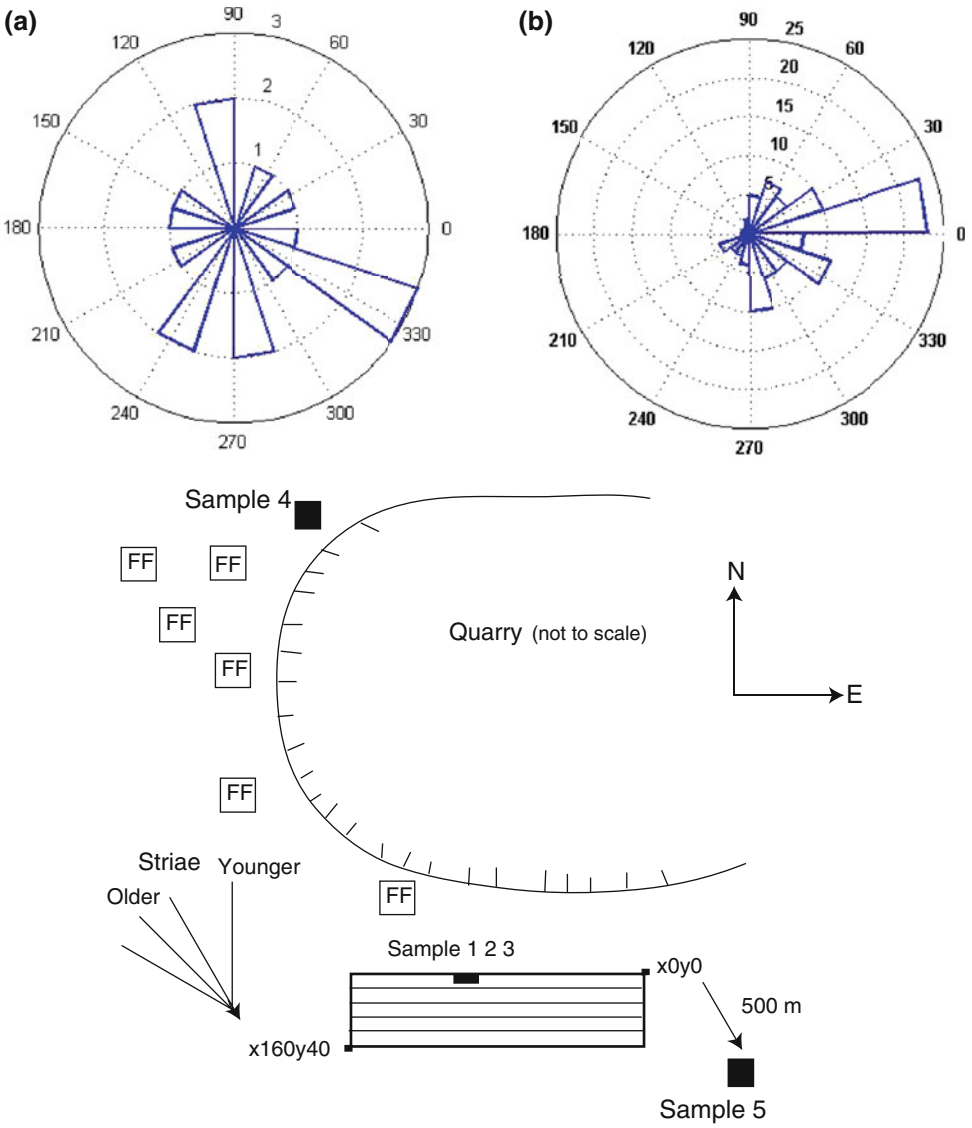

Fig. 7 Olunda, grid set-up with direction indicator shown. Rose diagram, **a** Direction of topographical features, **b** direction of fractures in the FF grids on a flat surface

Study of the overburden

In order to verify the results, test pits were excavated at Olunda and Dalby. This was not necessary at Bäckseda as there was a road cut between the face of the quarry and the study grid. Five 1 tonne samples were taken for analysis from Olunda and three from both Bäckseda and Dalby. Field sieving was used to separate the particles >200 mm and a 10 kg sample of the <20 mm material was taken back to the laboratory for sieving. The lithology of the 20–200 mm fraction was determined and each particle was weighed. As the total weight of each sample was 1 tonne and the total weight of the particles >200 mm was known, it was possible to establish the size distribution of the entire overburden, with the exception of the boulders.

In order to determine the thickness of the overburden, the ground surface was leveled prior to its removal. As the quarry expands in the grid direction and the overburden is removed, the surface is leveled again such that the thickness can be established. So far, the overburden has only been removed at the Olunda Quarry.

Fracture frequency

All discontinuities in the rock mass, joints, fractures and faults are referred to as fractures for simplicity and because it is not possible to distinguish any difference in the geophysical methods.

The fracture frequency was quantified at Olunda and Bäckseda, but not at Dalby for practical reasons. The method used consisted of studying the top surface of the

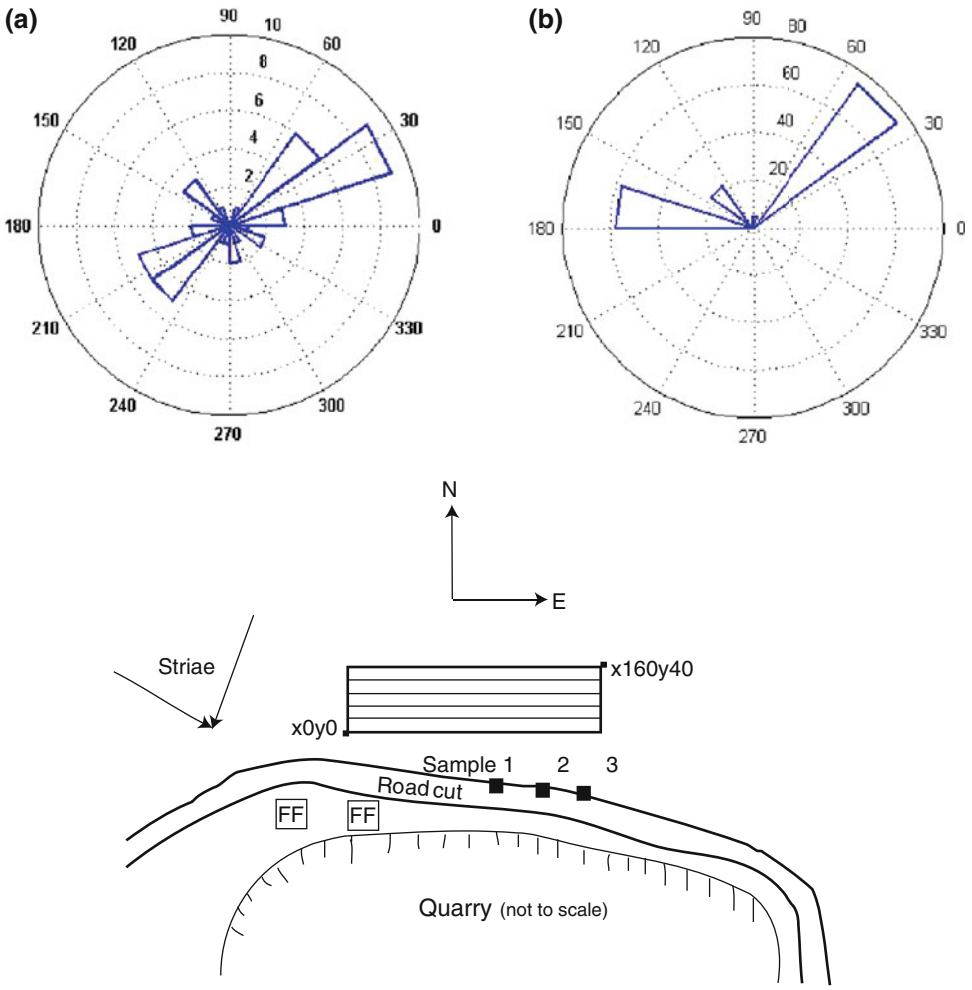

Fig. 8 Bäckseda, grid set-up, with direction indicator shown. Rose diagram, **a** Direction of topographical features, **b** direction of fractures in the FF grids on a flat surface

rock mass, close to the face of the quarry, in the area that had been cleared from overburden. The length and trend of fractures in 100 m^2 areas was established. The total length of all the fractures divided by the area gives an index value for the fracture frequency, FF Index.

$$\sum(\text{length } 1 + \text{length } 2 + \text{length } n)/\text{area} = \text{FF Index}.$$

This very quick and easy method only gives an estimation of the fracture frequency for vertical or sub-vertical fractures, not the horizontal ones. This was not done for Dalby due to the lack of a clean, smooth, rock surface after excavation of the overburden (Fig. 4). The rock mass at Dalby is so badly fractured that the excavated surface appears to be a field of angular boulders with no smooth rock surface for which fractures could be mapped. An alternative method could be to study the vertical rock face but safety and access considerations precluded this. However, numerous fractures could be seen at ca. 50 mm intervals in two to three preferred directions, suggesting the fracture frequency is generally at least more than double that of Bäckseda and in places up to 10 times more.

Data processing

The data was processed using *Res2dinv* (2D) and *Res3dinv* (3D), which uses automatic inverse numerical modeling techniques (inversion), with the finite difference or finite element method. In the inversion, the subsurface is divided into cells of fixed dimensions, the cell size normally increasing with depth. The resistivities are adjusted iteratively until an acceptable agreement between the input data and the model responses is reached (Dahlin 2001). However, large variations in the physically defined parameters may result in small variations in the observed data, hence damping and smoothness constraints are often included in the software to stabilize the process (Papadopoulos et al. 2007). In this study, the standard software values for damping and smoothness were used. The robust (L_1-norm) inversion option was used due to expected high contrasts in resistivity, and it has been shown that the robust inversion often gives a more stable result (Zhou and Dahlin 2003). *Erigraph* was used for calculating the NIP from the 2D-inversion results, which it is not possible to do with *Res2dinv* or *Res3dinv*.

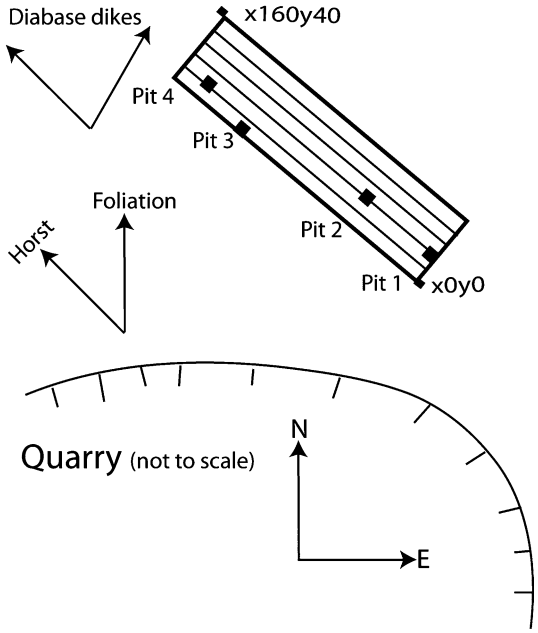

Fig. 9 Dalby, grid set-up, with direction indicator shown

Results and interpretation

As all the bedrock in Sweden is covered by glacial and postglacial sediments, it should be possible to distinguish two main units, bedrock (lower zone) and overburden (upper zone). Some difficulty does occur below the Quaternary shoreline where the till can be covered by clay, while above the fossil shoreline lakes and peat bogs may be present. The variations in resistivity for the upper zone (overburden) and lower zone (bedrock) varies extensively between the three sites (Table 1) and it is sometimes difficult to clearly distinguish an upper and lower zone in the results.

Geology of overburden

The overburden generally consists of glacial till which at Olunda is in part overlain by clay and at Dalby by sand.

Olunda overburden composition

The overburden at Olunda was sampled at five places (Fig. 7). Samples 1, 2, and 3 were taken from a trench dug parallel to the first line in the grid ($x100$, $y0$) and samples 4 and 5 about 500 m north and south of the grid, respectively.

Table 1 The different resistivity results from the three sites

Expected interpretation	Olunda (Ω m)	Bäckseda (Ω m)	Dalby (Ω m)
Overburden	<100–8,000	2,000–12,000	<200–14,000
Bedrock	At least 30,000	1,600	200
		6,000	400
			3,000

The trench was about 18 m long, 2–4 m deep, and 2.5 m wide. In the entire trench, clay (maximum thickness 1.5 m) covered 1–2 m of the till. The contact between the till and the clay consisted of a mélange zone some 1 m thick in which both clay and lumps of till/boulders are intermixed. Both Pits 4 and 5 were 1.5–2 m deep and exposed only a homogeneous till with a sandy, silty matrix.

The results of the lithological analysis of the 20–200 mm sized particles indicated approximately 90% has lithologies similar to the bedrock in the quarry. As seen in Table 2, these coarse particles composed 21% of the 1 tonne samples, except that from Pit 5, where the coarse particles amounted to 15% and the fines some 33%.

Bäckseda overburden composition

The thickness of the till varied from about 2–6 m. Along the road cut (Fig. 8), five diffuse, sub-horizontal layers could be distinguished in the till. The road cut, as well as the rock surface, sloped to the east and the layers of till appeared one under the other along the extent of the exposure. Samples were taken from the three middle layers (Samples 1, 2, 3 from layers 2 to 4, respectively). The uppermost layer is about 0.5 m thick in which a soil profile is well developed. It was not possible to sample the lowermost layer as it was at the edge of the face of the quarry.

The till is generally massive. The matrix is predominately composed of sand and silt. Several of the clasts are oriented with their longest axis in a vertical position. There are a few, folded lenses of sorted silt and sand, primarily in layer two. The clast frequency is greater in layer three than in the other layers and the uppermost part of layer three consists of a boulder string.

The lithology of the clasts from the three samples indicated the composition differed from the rock in the quarry. As seen in Table 2, the weight% of the coarse particles in the three samples varied between 17 and 27% (Table 2) and the silt and clay fraction from 19 to 26%.

Dalby overburden composition

At Dalby, the overburden was studied in four pits within the grid (Fig. 9). The upper 0.4–0.9 m in pits 1 and 3 consisted of sand. Although generally massive, the till also contained some grey clay-rich lenses, sand lenses and coarse clasts just above the bedrock. It was difficult to determine the bedrock surface due to the highly fractured character of the rock.

Table 2 Weight% for coarse particles and fine material for the three sites. Sample size are 1 tonne, except Dalby sample 1.2 and 2.3, which are 500 and 250 kg, respectively

Sample	6–20 cm (kg)	2–6 cm (kg)	Weight of clasts (kg)	% coarse particles	% clay and silt
Olunda					
1	113	90	203	20	21
2	151	81	231	23	17
3	175	80	254	25	20
4	151	81	231	23	12
5	104	48	152	15	33
Bäckseda					
1	74	98	170	17	26
2	157	115	272	27	21
3	123	90	213	21	19
Dalby					
1.1	–	–	–	9	21
1.2	–	–	–	28	16
2.3	–	–	–	25	9

The first two samples were taken from Pit 1 at 1.2 m and 2–2.5 m depth. The third sample was taken in Pit 2 at 1 m depth. A small diabase dyke was exposed at the bottom of Pit 2. No samples were taken from Pits 3 and 4, which were excavated to establish the depth to bedrock. This was at approximately 1.5 m in Pit 3 but could not be distinguished below the topsoil in Pit 4.

The composition of the fragments in the till is almost exclusively the same as the material exposed in the rock quarry. The weight% of the coarse particles varied between 8.1 and 28% and the silt and clay fraction between 8.9 and 21% (Table 2).

Fracture frequency results

The FF Index was measured in grids of 100 m^2, six at Olunda and two at Bäckseda. The mean for Olunda is 0.7 m/m^2 and for Bäckseda 2.0 m/m^2 (Table 3). As noted above, the fracture frequency could not be measured at Dalby but was assessed to be considerably higher.

Table 3 Fracture frequency index (FF index)

Grid	FF index
Olunda	
1	0.5
2	0.9
3	0.7
4	0.8
5	0.7
6	0.9
Bäckseda	
1	1.7
2	2.4
Dalby	
1	10 × Bäckseda

ERI and IP results

Both the ERI and IP results are presented as horizontal and vertical slices. All the graphs originate from the same inversion. The NIP is presented in vertical slices from the 2D-inversion as *Res3dinv* does not yet support normalized IP.

- ERIH: horizontal slices with x, y coordinates, the depth, z, represents an average of 4 m but is referred to, for simplicity, as the highest integer value for the slice;
- ERIV: vertical slices with x, z coordinates, each slice is an average of 4 m in the y direction referred to, for simplicity, as the highest integer value for the slice;
- IPH: same coordinate system as for ERIH;
- IPV: same coordinate system as for ERIV;
- NIP: vertical slices with x, z coordinates. Note that they are not an average in the y direction but the y coordinate follows the grid lines coordinates exactly.

The orientation of the horizontal resistivity diagrams is dependent upon the direction in which the measurements are made in the field (Figs. 7–9). In the case of Olunda, north is upwards and in Bäckseda, north is down while for Dalby, down is toward N40° and right is N310°. As can be seen from Table 1, the electrical resistivity at the sites varies considerably. Olunda has the lowest and Dalby the highest fracture frequency.

Olunda

Electrical resistivity imaging

The inversion results (Fig. 10) indicate the upper and lower zones, although the boundary between these is not clear cut, ranging from 8,000 to 13,000 Ωm. In some places, the upper zone is lacking.

The upper zone can be divided into two parts. The first consists of pockets at the surface with resistivities <100 Ωm, below which the resistivities are up to 8,000 Ωm. The lower zone has a high resistivity in the upper part (13,000 Ωm), which increases with depth such that at about 10 m it is over 30,000 Ωm. The pockets <100 Ωm could represent clay with a high water content while the remainder is interpreted to be till. The moderate values of the resistivity, normally around 1,500, but up to 8,000 Ωm, suggest that the till is moderately conductive.

The boundary between the upper and lower zones is an undulating surface (Fig. 10b), varying in depth.

In the lower zone, which is 6–10 m wide and trends NS, there is one vertical low resistivity section, at a distance of 45 m (Fig. 10). Several less predominant vertical deviations in the resistivity are also evident, trending about N045° (Fig. 10a) and with a dip of 65°SE (Fig. 10b). This high resistivity zone is interpreted to be bedrock, with very little water and few conductive minerals in the rock mass. This in turn would indicate that there are few fractures and that the rock is not weathered, although the variation in the resistivity could reflect a slight variation in fracture frequency. It is common in glaciated regions that horizontal relaxation joints form with higher frequency near the ground surface and decrease with depth due to unloading (Nichols and Collins 1991).

The undulating contact between the upper and lower zones is interpreted to be the bedrock surface at between 8,000 and 13,000 Ωm, which can mean an uncertainty of at least 1 m in the predicted bedrock surface position. In places, the bedrock crops out but in general it is about 2–3 m below the ground surface and in the east end ($x0$–$x10$, y all, $z7$ Fig. 10a), of the grid reaches a maximum of about 7 m.

The low resistivity zone at $x45$ is interpreted to be a vertical fracture zone (Fig. 10b) trending NS (Fig. 10a) with a width of between 6 and 10 m. The low resistivity suggests that this zone could be rich in water or altered conductive minerals. There is a valley in the resistivity (primarily at $y12$–$y28$ of the grid), which is interpreted to be a system of parallel fractures.

Comparison with samples

The overburden was interpreted to be till with a high content of water or clay. This was confirmed as the trench excavated for samples 1, 2, and 3 filled with water one day after excavation. The contact between the overburden and bedrock consisted of a 1 m thick sheared zone of clay and till, which explains why it was very diffuse in the resistivity images. The difference in altitude before and after the removal of the overburden was between 0 and 7 m. The thickest part was in the eastern end of the section, consistent with the geophysical interpretation.

The NS or N315° fracture trends suggested by the interpretation were not confirmed (Fig. 7b), probably due to the study being carried out on the rises rather than the lows in the bedrock. Measurements in the grid area after the overburden was removed showed that the trend of the predominant topographical features in the undulating bedrock had several different directions (Fig. 7a). These agreed quite well with the interpretation of a predominant set of fractures trending N315°.

The study indicated that this method can provide a realistic estimation of the thickness and volume of the overburden. The calculations for one of the lines ($x30$–$x140$) indicated 122 m^2 while after the leveling of the cleared surface the overburden was determined as 109 m^2. The high resistivity of the bedrock indicates a low fracture frequency, consistent with the low FF Index. The rock mass appears to be homogeneous and sound with the possible exception of the NS trending fracture zone($x45$, y all, z all), which appears to be a few metres wide and may be extensively crushed, weathered and containing a large amount of water.

Bäckseda

Electrical resistivity imaging

In general, the resistivity at Bäckseda lacks the extreme low values (Fig. 11) that occur at both Olunda and Dalby, varying from 400 to 15,000 Ωm. The contact between the upper and lower zone is normally at less than 4 m deep, although in some places it was up to 7 m (Fig. 11a).

The upper zone (Fig. 11b) can be divided into two parts, with the upper layer having a slightly lower resistivity (around 2,000 Ωm) than the lower layer.

The lower zone is characterized by large homogeneous areas with gradual transitions, 2,000–6,000 Ωm. In general, the lower zone becomes more homogeneous with depth. The ERIH (Fig. 11a) reveal the occurrence of three anomalously low resistivity areas (400 Ωm).

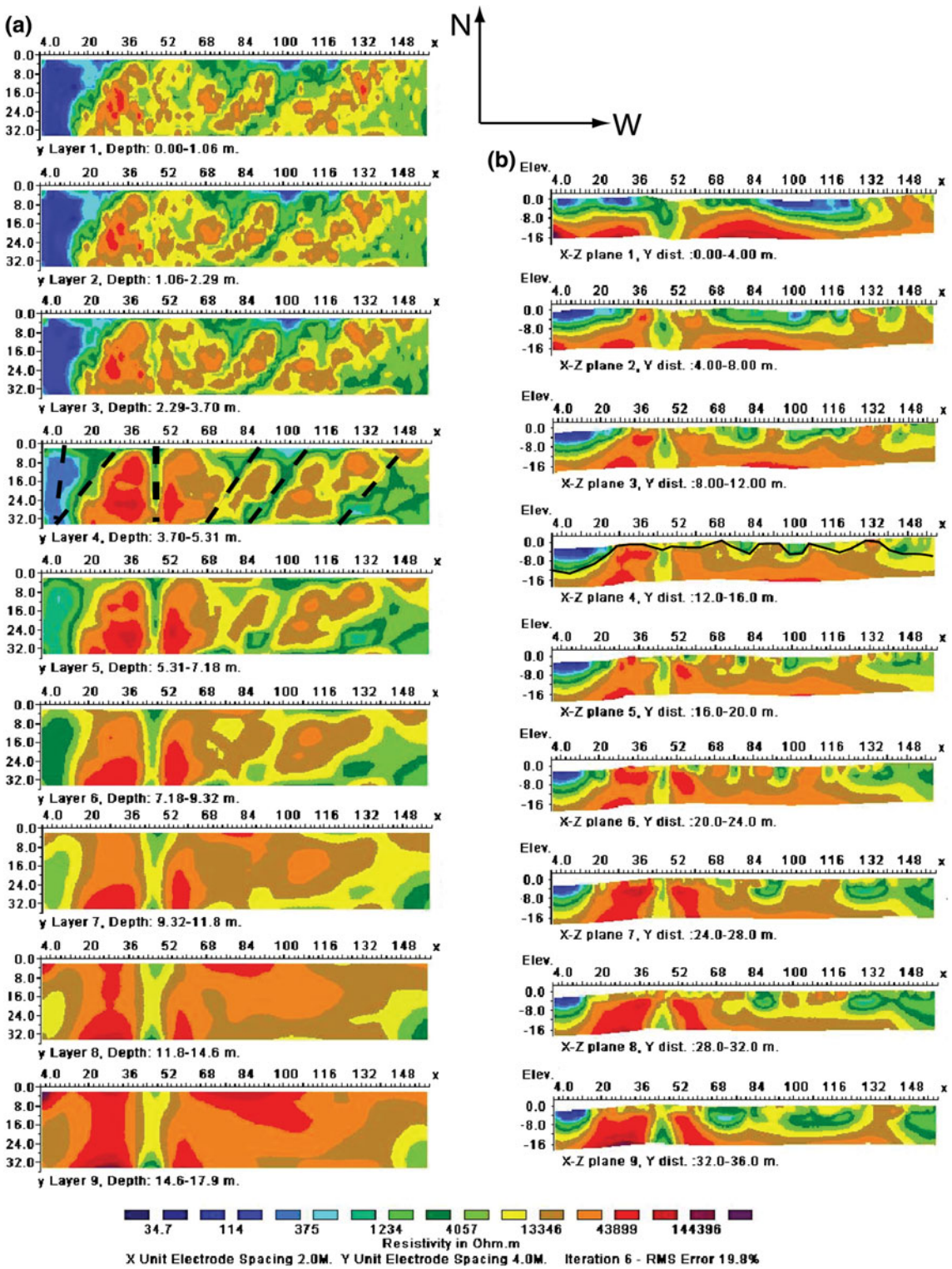

Fig. 10 Olunda electrical resistivity imaging from 3D inversion, direction indicator shown at the *top*; **a** *horizontal slices*, ERIH, interpretation of weakness zones are added to graph four from the top; **b** *vertical slices* from, ERIV, interpretation of the thickness of the overburden is added to graph four from the top

1. Line A, from 5 to 11 m depth, is quite straight and trends N320° ($x90$, $y40$, $z5$–$z11$ to $x130$, $y0$, $z5$–$z11$).
2. Lines B and C form an "s" shape. Line B, trending N030°, is quite short but extends downward to 21 m depth ($x98$, $y0$, $z5$–$z21$ to $x110$, $y16$, $z5$–$z21$). Line C

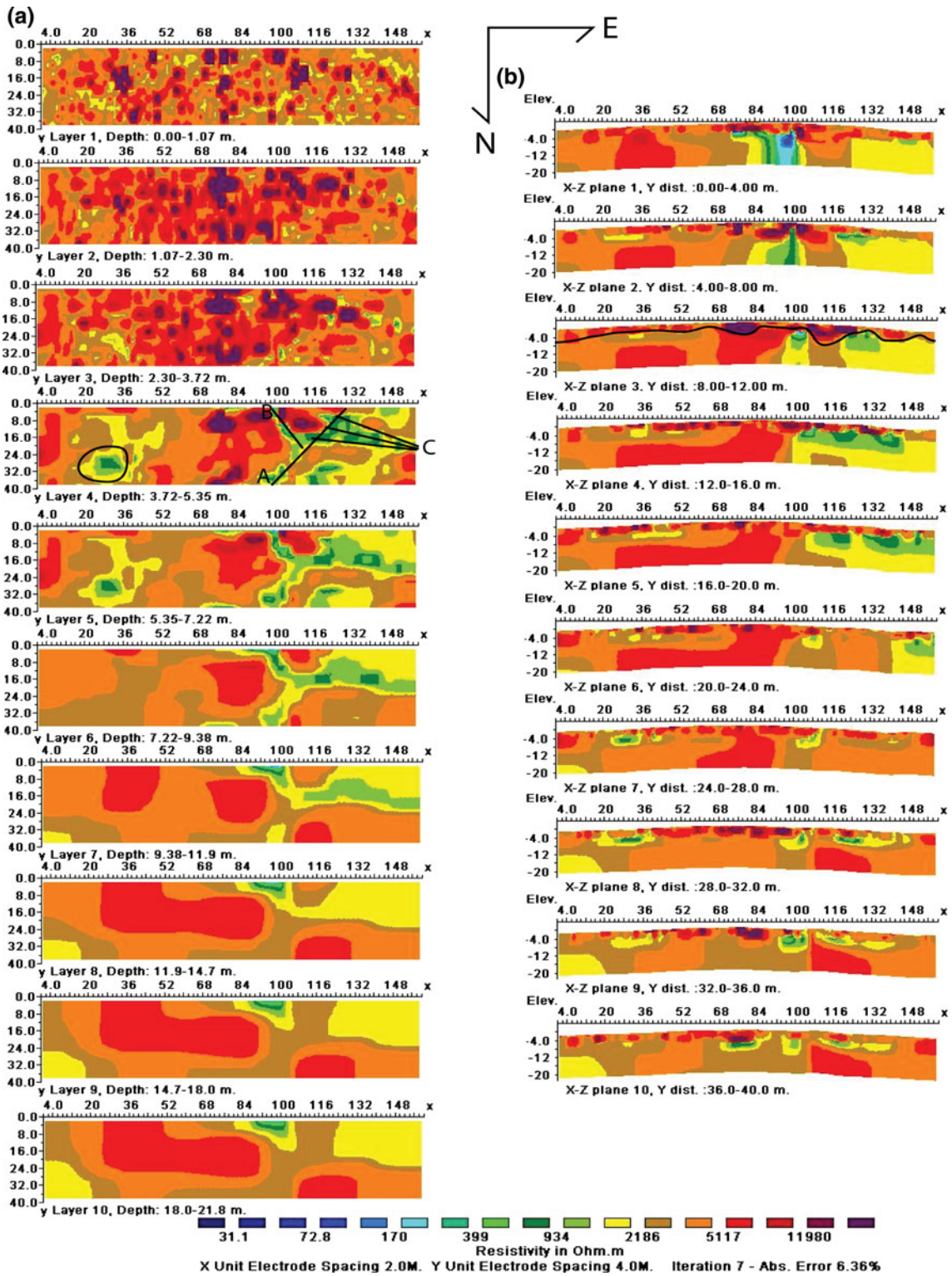

Fig. 11 Bäckseda Electrical Resistivity Imaging from 3D inversion, direction indicator shown at the *top*; **a** *horizontal slices*, ERIH, interpretation of weakness zones/anomalies are added to graph four from the top; **b** *vertical slices*, ERIV, interpretation of the thickness of the overburden is added to graph three from the top

occurs from 5 to 11 m depth and has a much more variable trend, shown as different lines in Fig. 11.

3. A circular anomaly occurs from 5 m to 7 m depth and has its focus at *x*28, *y*28, *z*5–*z*7.

IP and normalized IP

The IPV and IPH results (Fig. 12) show a similar pattern to the ERIH and ERIV (Fig. 11), with a higher IP effect in the

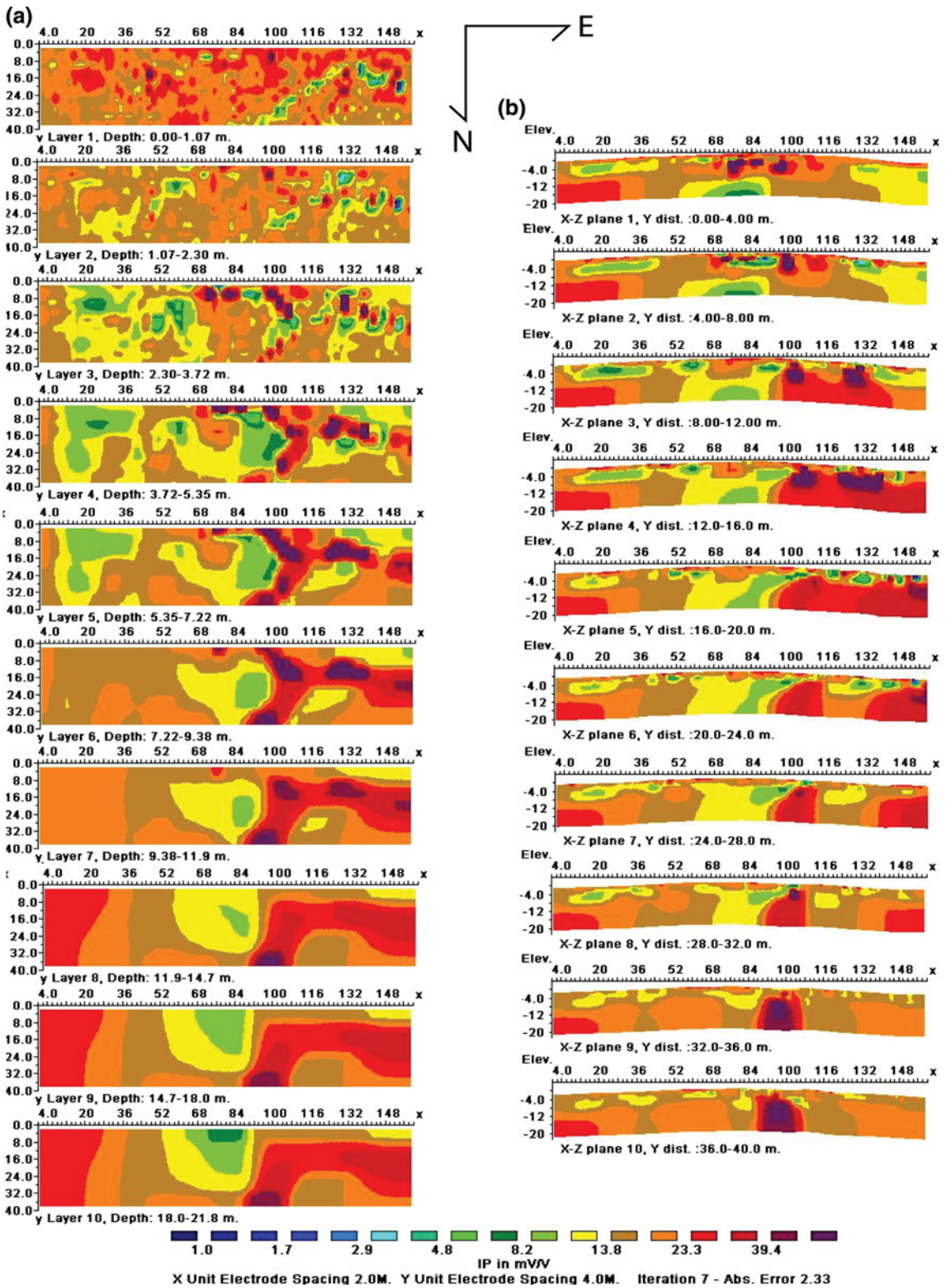

Fig. 12 Bäckseda-induced polarization from 3D inversion, direction indicator shown at the *top*; **a** *horizontal slices* IPH; **b** *vertical slices*, IPV

same area as lines A, B, and C. The NIP (Fig. 13a) shows little difference in the vertical direction (i.e. no upper and lower zone) but there are three pronounced anomalies with maximum normalized chargeabilities of ∼1 mS/m, at *x*80, *y*4, ∼0.3 mS/m, at *x*100 almost all *y*, and ∼0.4 mS/m, at *x*130, *y*12–*y*20. These are located at about the same places

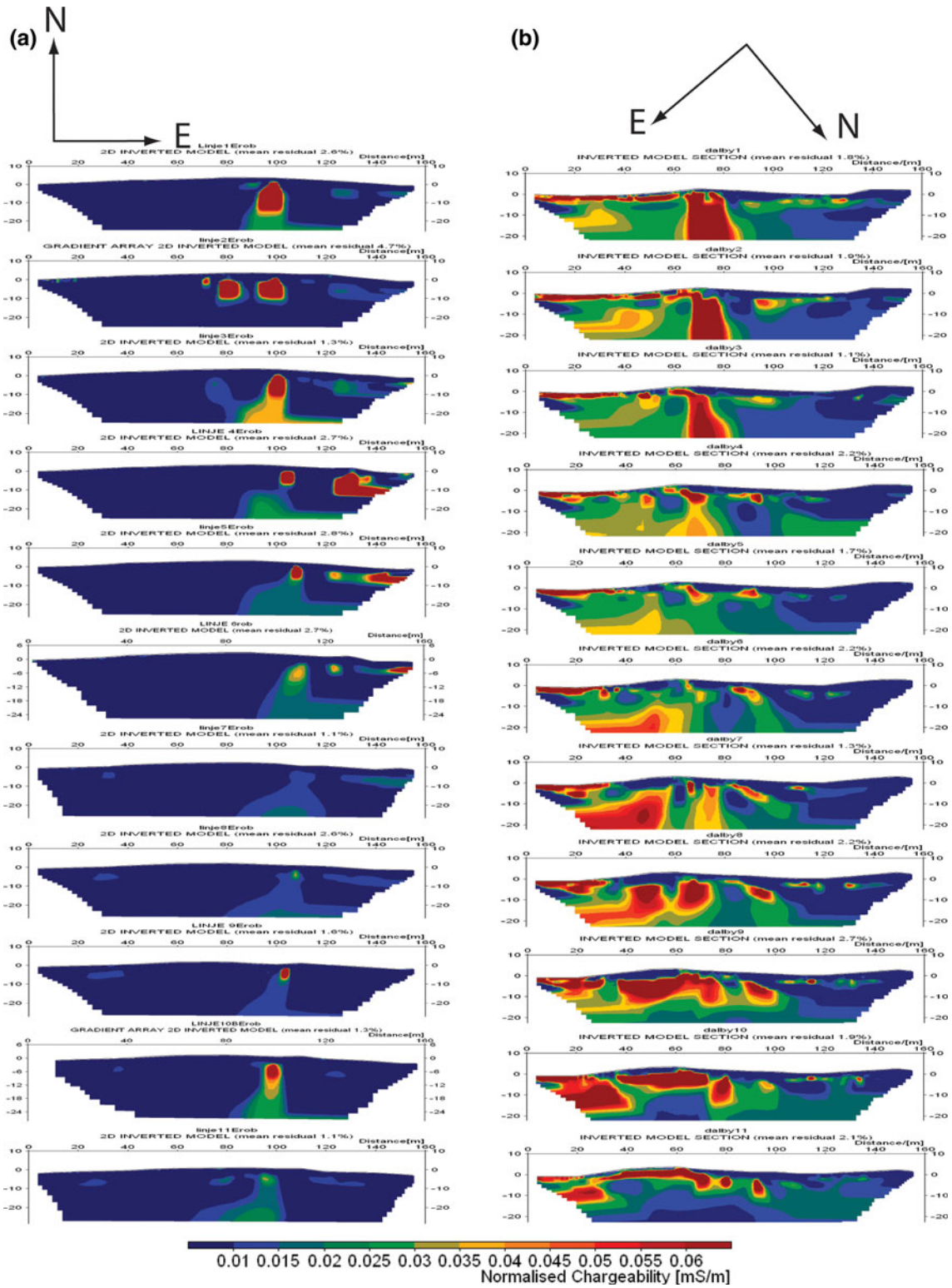

Fig. 13 Normalized induced polarization from 2D inversion, direction indicator shown at the *top*, line 1 at the top and line 11 at the bottom; **a** Bäckseda, **b** Dalby

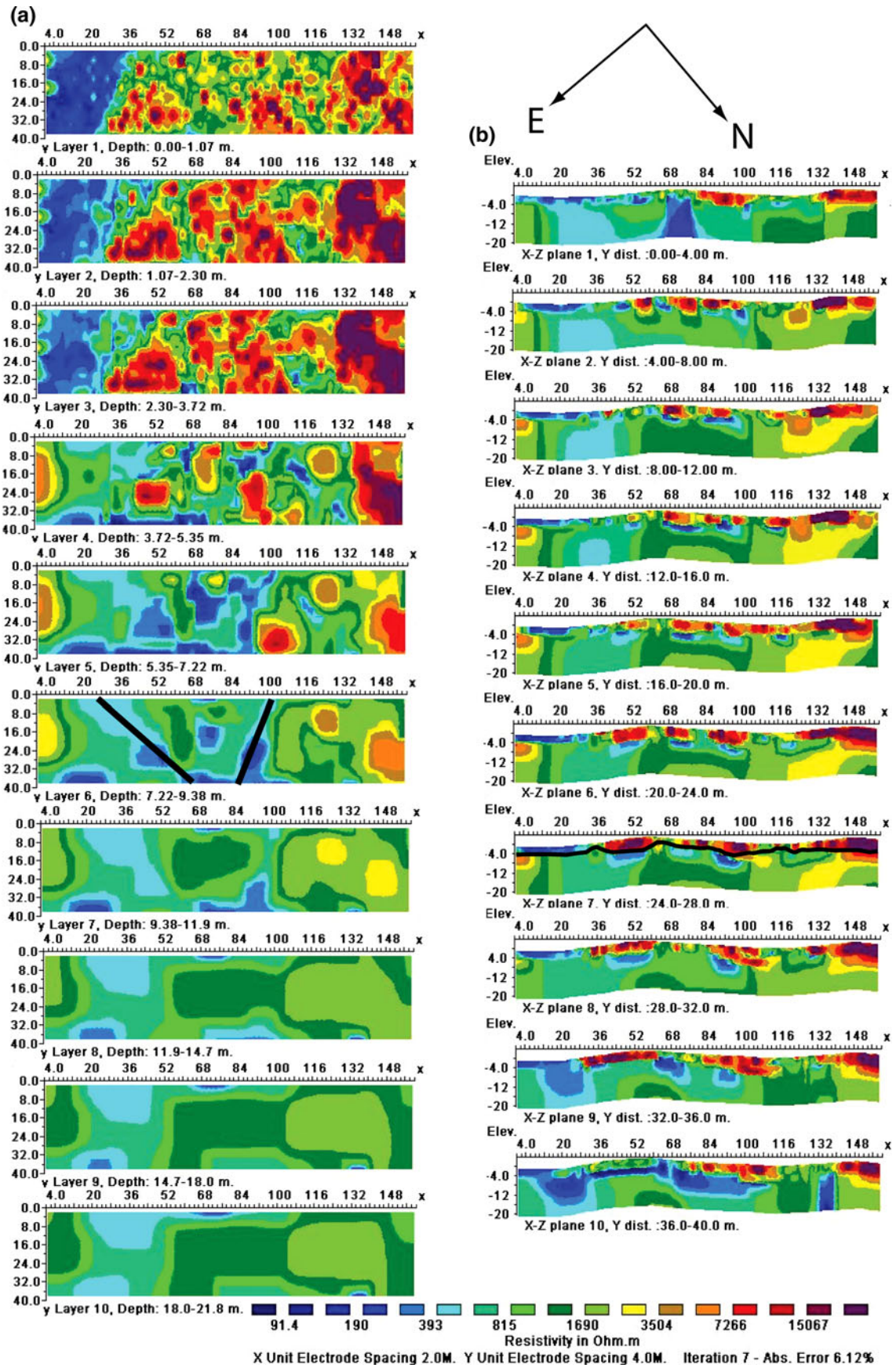
(a)
y Layer 1, Depth: 0.00-1.07 m.
y Layer 2, Depth: 1.07-2.30 m.
y Layer 3, Depth: 2.30-3.72 m.
y Layer 4, Depth: 3.72-5.35 m.
y Layer 5, Depth: 5.35-7.22 m.
y Layer 6, Depth: 7.22-9.38 m.
y Layer 7, Depth: 9.38-11.9 m.
y Layer 8, Depth: 11.9-14.7 m.
y Layer 9, Depth: 14.7-18.0 m.
y Layer 10, Depth: 18.0-21.8 m.
(b)
E
N
X-Z plane 1, Y dist. :0.00-4.00 m.
X-Z plane 2, Y dist. :4.00-8.00 m.
X-Z plane 3, Y dist. :8.00-12.00 m.
X-Z plane 4, Y dist. :12.0-16.0 m.
X-Z plane 5, Y dist. :16.0-20.0 m.
X-Z plane 6, Y dist. :20.0-24.0 m.
X-Z plane 7, Y dist. :24.0-28.0 m.
X-Z plane 8, Y dist. :28.0-32.0 m.
X-Z plane 9, Y dist. :32.0-36.0 m.
X-Z plane 10, Y dist. :36.0-40.0 m.
91.4 190 393 815 1690 3504 7266 15067
Resistivity in Ohm.m
X Unit Electrode Spacing 2.0M. Y Unit Electrode Spacing 4.0M. Iteration 7 - Abs. Error 6.12%

◀ **Fig. 14** Dalby electrical resistivity imaging from 3D inversion, direction indicator shown at the *top*; **a** *horizontal slices*, ERIH, interpretation of weakness zones/anomalies are added to graph six from the top; **b** *vertical slices*, ERIV, two different interpretations of the thickness of the overburden is added to graph seven from the top

as the low resistivity anomalies (Fig. 11). They are generally <4 m from the ground surface but can extend to 10–15 m depth.

Interpretation of Bäckseda

The upper zone is interpreted as till, with its maximum thickness (Fig. 11a) at *x*80 all lines and *x*110, *y*4–y12. As the resistivity is relatively high, it is probably very dry with a high frequency of coarse particles and low silt and clay content. The resistivity in the upper zone could be divided into two layers, which could reflect different till units. However, as the site is at the top of a hill and the rock quarry walls are 40 m high, the groundwater level in the overburden close to the quarry is expected to be very dry, which may account for the high resistivities. This is also seen in the IP (Fig. 12) in the upper layer, but is not seen at all in the NIP (Fig. 13a).

The resistivity in the upper part of the bedrock is lower than in the till but increases with depth to about the same as the till. The low resistivity suggests that the upper part of the rock mass is fractured and that the fractures are filled with conductive material. However, similar to the interpretation at Olunda, there is a decrease in horizontal fractures with depth and they are tighter and less water bearing.

The low resistivity in parts (lines A, B, and C) and the corresponding anomaly for the IP and NIP, could indicate a more highly fractured zone in the bedrock filled with clay, graphite or water. There could also be pockets of conductive soils, especially in the sub-circular area which is only visible down to 7 m and could therefore be the junction of the bedrock and till. However, the sub-circular area does not correspond to the anomalous areas in the NIP.

Dalby

Electrical resistivity imaging

Dalby is more complex than the other two sites. Although there is still an upper and lower zone, these are not homogenous.

The upper zone can be divided into two parts with different resistivities (Fig. 14).

1. A low resistivity part <200 Ωm, covering the entire left part of the grid, from the surface down to approximately 3.5 m.
2. A very high resistivity part 7,000 to 14,000 Ωm consisting of discontinuous "islands" surrounded by roughly linear depressions of low resistivity (Fig. 14a). Two different (N355° and N064°) linear systems seem to recur, delineating the "islands" which are more frequent and smaller in the upper 1 m and become fewer and larger with depth.

The lower zone at Dalby (Fig. 14) has relatively low resistivities, 100–3,000 Ωm (Table 1). Some vertical anomalies with particularly low resistivities were identified in the ERIV (Fig. 14b), while there is a zone with a slightly higher resistivity at *x*132, *y*12–*y*28, *z*4–*z*20.

IP and normalized IP

The IPV (Fig. 15b) results also suggest an upper and lower zone. The upper zone is characterized by small patches of high to extremely high IP values with abrupt transitions in values. This is also seen in the IPH (Fig. 15a) for *y*1. The lower zone is characterized by large bodies with moderate IP values with gradational transitions. There is also a section with lower chargeability in the IPV and IPH results, part of which corresponds to an anomaly in the ERIV.

In the normalized IP profiles (Fig. 13b), the upper zone can be divided into two parts with higher and lower values. The bedrock surface is interpreted to be the contact between the upper and lower zones. This is generally at about 2–4 m, although it can be higher. In the NIP profiles, the bedrock surface may increase to 8 m, but this is not supported by either the IPV profile or the ERIH and ERIV profiles. In one area (*x*0–*x*25), the high NIP values and the extremely low ERI values suggest the overburden is more chargeable and less resistive. This may be related to pore water or clay content. At *y*20–*y*40, the high NIP occurs as semi continuous, sub-horizontal layers (Anomaly 1). Another notable area, with high NIP values is at *x*70–*x*80, *y*0–*y*8, *z*0–*z*20 (Anomaly 2).

Interpretation of Dalby

As discussed above, part of the upper zone is hard to interpret (Fig. 14). This part of the section has extremely high ERI values when compared with most tills (Palacky 1989) although the patchy pattern in the ERIH, ERIV, IPV, and IPH profiles suggests an inhomogeneous material. The thin patches of high NIP values and the low ERIV values (Anomaly 3) may mark the overburden/bedrock surface. This is thought to represent small isolated basins in the "true" bedrock surface where groundwater is trapped for longer periods of time than elsewhere in the surroundings. In these areas, both the lower part of the overburden and the fractures in the upper part of the bedrock will be

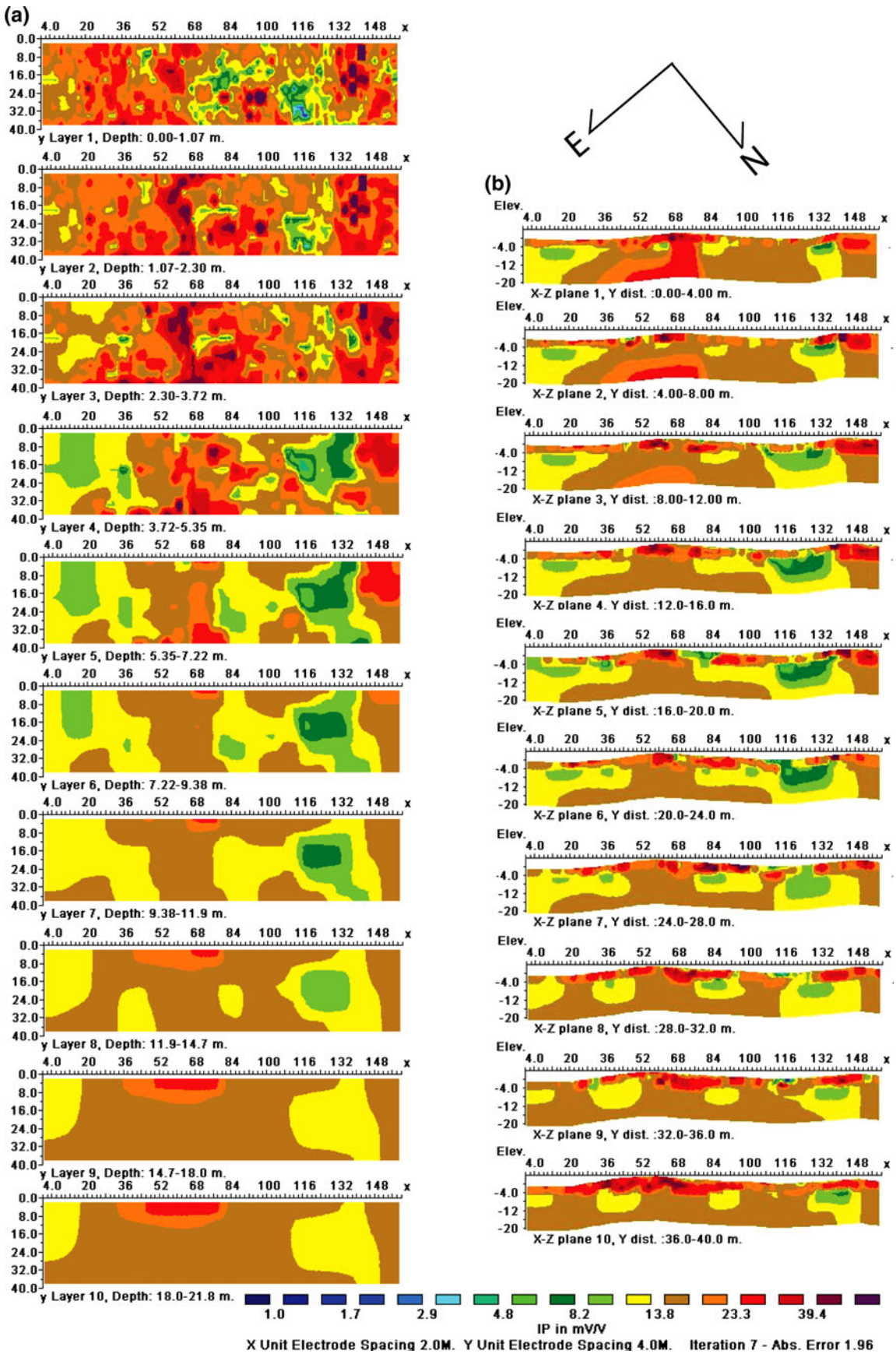
(a)
y Layer 1, Depth: 0.00-1.07 m.
y Layer 2, Depth: 1.07-2.30 m.
y Layer 3, Depth: 2.30-3.72 m.
y Layer 4, Depth: 3.72-5.35 m.
y Layer 5, Depth: 5.35-7.22 m.
y Layer 6, Depth: 7.22-9.38 m.
y Layer 7, Depth: 9.38-11.9 m.
y Layer 8, Depth: 11.9-14.7 m.
y Layer 9, Depth: 14.7-18.0 m.
y Layer 10, Depth: 18.0-21.8 m.
E
N
(b)
X-Z plane 1, Y dist. :0.00-4.00 m.
X-Z plane 2, Y dist. :4.00-8.00 m.
X-Z plane 3, Y dist. :8.00-12.00 m.
X-Z plane 4. Y dist. :12.0-16.0 m.
X-Z plane 5, Y dist. :16.0-20.0 m.
X-Z plane 6, Y dist. :20.0-24.0 m.
X-Z plane 7, Y dist. :24.0-28.0 m.
X-Z plane 8, Y dist. :28.0-32.0 m.
X-Z plane 9, Y dist. :32.0-36.0 m.
X-Z plane 10, Y dist. :36.0-40.0 m.
1.0 1.7 2.9 4.8 8.2 13.8 23.3 39.4
IP in mV/V
X Unit Electrode Spacing 2.0M. Y Unit Electrode Spacing 4.0M. Iteration 7 - Abs. Error 1.96

◀ **Fig. 15** Dalby-induced polarization from 3D inversion, direction indicator shown at the *top*; **a** *horizontal slices*, IPH; **b** *vertical slices*, IPV

moister than in other areas (Fig. 16a). In this case, this could mark the point between the disturbed upper part of the bedrock and the "true" intact part of the bedrock (Fig. 16b). In the disturbed portion, there would be a much more open nature to the material which is not filled with matrix and is situated above the groundwater level, hence would be very dry yielding extremely high resistivity. However, this would mean that the bedrock is above the groundwater level, which is unlikely in view of the close proximity to the rock quarry. Alternatively, the bedrock could have been dried in the upper part by wind-enhanced evaporation (Fig. 16c). The anomaly could also mark a salt-enriched zone.

Based on the IPV, IPH and NIP profiles, Anomalies 1 and 2, the bedrock is interpreted to be highly variable with several different rock types occurring. This is not consistent with the ERIV and ERIH results, which suggest relatively homogeneous highly fractured material.

1. Anomaly 1 is interpreted to be a diabase dyke or amphibolite zone trending nearly parallel to the study profiles (N350° compared with the dyke which appears to strike about N305° and dip about 45° towards the NE). It therefore cuts the profiles at different depths in the different profiles. This would agree with the trend of both the horst and the youngest set of dykes in the area.
2. Anomaly 2 is interpreted to be a diabase dyke that strikes parallel with the short axis of the grid N040° and vertical dip. This may belong to the next youngest dykes that are reported to trend NNE–SSW and dip steeply to the west. It is surprising that the dyke does not continue through all the profiles, as it would be assumed this would be relatively continuous along the strike. There is no clear explanation for this, although it is possible that it is tectonically offset. Ringberg (1980) has noted how much dykes vary in thickness, which could account for their seemingly discontinuous trend.

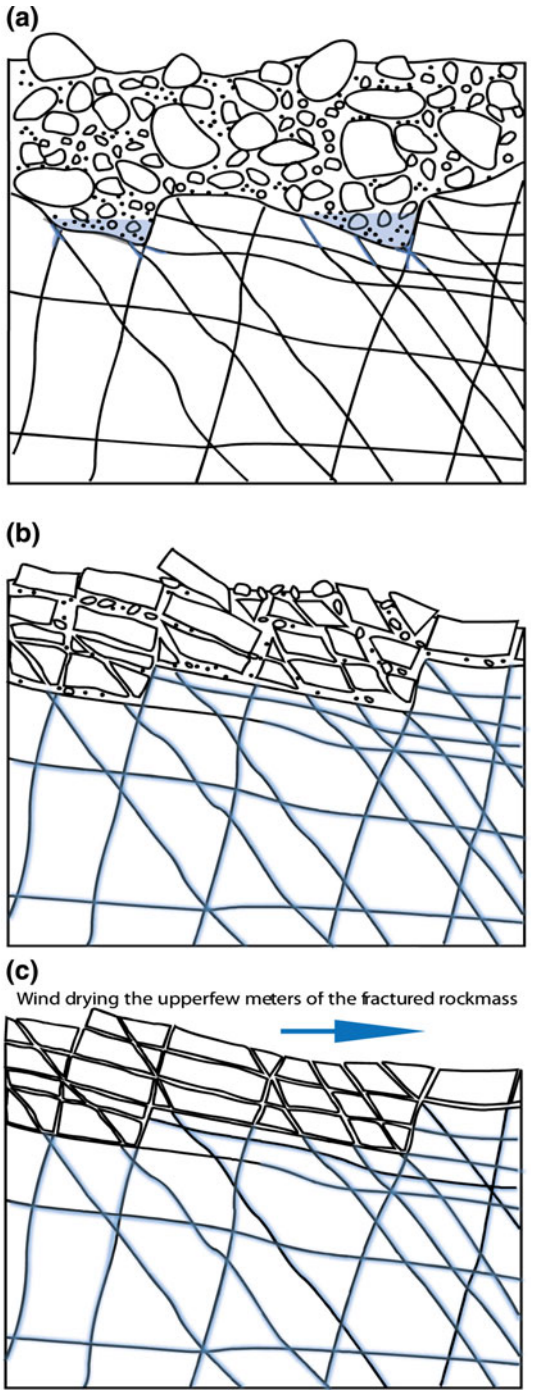

Fig. 16 Models for different interfaces, **a** pockets in the interface retaining water, **b** the interface between overburden and bedrock, **c** wind drying of the upper few meters

Comparison with samples

The depth to bedrock was interpreted to be 2–4 m over the entire area. The excavation pits suggested it varied between 0 and 2.5 m (Fig. 9), although at Dalby, it was difficult to determine because of the fractured nature of the rock. The low resistivity (left) part of the grid contained only 9% coarse particles and 21% fine material, which could explain the ERI and NIP effect. The high values at the contact between the upper and lower zones in the NIP (Anomaly 3) corresponding to some of the low resistivity areas in the ERIV, are not clearly understood. This may be elucidated when the area is excavated and can be inspected. Anomaly 1 was interpreted as a diabase dyke or an amphibolite dyke. Several dykes are observed in the rock quarry with similar

orientations. Some are folded and faulted. Again, this can only be confirmed when the quarry has expanded.

Anomaly 2 was interpreted as a discontinuous diabase dyke striking N040°. There is a small patch with very high NIP values just at the top of the lower zone but it does not continue downward in the section as would be expected for a dyke.

Discussion

Interpretation of the geophysical profiles requires knowledge of the general geology of the area. Undertaking 3D inversion gave a much better basis for the interpretation than only 2D inversion, increasing the reliability as horizontal slices are also available. The results of the ERIH, ERIV, IPV, IPH, and NIP also showed that using different methods increases the understanding of the subsurface.

Examples where the interpretation has been based on several profiles include:

- Lines A, B, C at Bäckseda would not have been interpreted as lines if the ERIH had not been available.
- With the IPH and the NIP, lines A, B, C at Bäckseda were better constrained.
- The diabase dykes, Anomalies 1 and 2, at Dalby would not have been interpreted as such if the NIP had not been available.
- The till thickness would have been much more difficult to interpret at all three sites if the ERIH had not displayed the patchy pattern which seems typical for till.
- The NS trending fracture zone at Olunda was not visible in the single lines, but with the ERIH and ERIV graphs it was very clear.

This shows that combining the data from parallel 2D profiles is equivalent to a 3D roll-along process, which works very well in practical applications. Compared with establishing a full 3D grid, it is not only much less time consuming and costly, but also more practical in many parts of Sweden.

The geophysical characteristics of the overburden at the three sites are quite different. The low to moderate resistivity of the till at Olunda, <8,000 Ωm, is considered to be due to the high groundwater level and the presence of clay minerals in the overburden. The resistivity at Bäckseda and Dalby reaches 12,000 Ωm (higher than the bedrock) due to the extremely dry conditions at these two sites, but the constraints are not clear. For Dalby, it is suggested that part of the overburden might not be till, but very fractured rocks which were not incorporated in the glacier (Fig. 16); the lack of matrix resulting in a drier material, possibly exacerbated by wind evaporation.

At Bäckseda, there were at least five different till layers, but this is not evident in the results, possibly because the 2 m electrode interval is too great. A 0.5 m spacing is probably required.

The study indicated that it is possible to estimate the quantity of overburden, which exists in an area using ERI in parallel profiles and the 3D inversion technique, but for some areas additional geophysical measurements (e.g. seismic refraction) could better constrain the estimations when the resistivity of the overburden is similar to that of the bedrock. The zones of lower resistivity at the junction between the overburden and bedrock seen in both Bäckseda and Dalby could be explained by groundwater or fine material caught in isolated basins in the undulating bedrock/overburden contact (Fig. 16a).

The resistivity for the bedrock is very variable between the sites. The limited number of fractures at Olunda means that mineralization has not occurred. At Dalby, diabase dykes were identified by combining the results from the resistivity and IP. Identification of variations in the rock mass is important not only for maintaining uniform aggregate quality, but because it may also have implications for the chemical suitability of the crushed product for various construction purposes.

Conclusions

1. Geophysics can be a valuable tool for the quarrying industry. The results show that geoelectrical imaging is well suited for determining:
   a. the fracture frequency of the rock mass; low resistivity reflecting high fracture frequency. This is important when opening a rock quarry as few fractures may lead to difficulty in fragmentation during blasting and result in additional costs for aggregate production.
   b. the homogeneity of the rock mass, weathered zone, and changes in lithology.
   c. the volume of overburden—this affects the viability of the quarry.
2. When conducting a survey with ERI using the software *Res3dinv*, it is important to carefully consider the grid setup. In the case of both Olunda and Bäckseda, the lines have been to the left (i.e. standing at $x0y0$ facing $x160y0$, the next line is to the left). The drawback with this is that the software switches the direction, therefore north is downwards in one of the graphs and not upwards, which would be the most logical way. At Dalby, the survey was conducted with the lines to the right, giving a more logical view of the results. Geoelectrical imaging with 2 m intervals

between electrodes did not give enough detail to conclude the composition of the overburden; a spacing of 0.5 m would be more appropriate.

3. Combining parallel 2D-sections can be considered as a 3D roll-along process that works very well in practical applications, especially where establishing a full 3D grid would not be realistic due to terrain and vegetation. The 3D horizontal slices gave valuable information about the direction of the weaker zones. A combination of electrical resistivity, IP and normalized IP made it possible to be more precise in the interpretation of the soil rock interface, homogeneity of the rock mass and orientation of fractures.
4. Using different geophysical methods is beneficial during prospecting for rock quarries as it can give a more complete picture of the rock mass characteristics, fracture frequency and homogeneity, than just a few drill holes. It is also a valuable tool when planning the expansion of the quarry. The overburden thickness can be determined in advance, allowing for better estimation of the cost of removal; and the fracture orientation can be assessed which can assist in determining the direction of excavation that yields the most stable rock faces.
5. The study has reported the use of ERI together with IP to assess factors affecting the development of three rock quarries in Sweden. In other cases, interpretation could be supported by other geophysical methods such as seismicity, drilling, or trenching. Attention is also drawn to the importance of having profiles against which the geophysical data can be assessed.

Acknowledgments The work behind this paper was funded by The Swedish Research Council for Environment, Agricultural Sciences, and Spatial Planning (Formas). Thanks to Björn Eliasson at Skanska Sverige AB, Asfalt och Betong Mellansverige; to Magnus Tillman at Hagéns Åkeri and to NCC Roads; and to Björn Linné at Sydsten, for allowing us to use the quarries as test sites.

References

Aaltonen J, Olofsson B (2002) Direct current (DC) resistivity measurements in long-term groundwater monitoring programmes. Environ Geol 42:662–671

Arnbom JO, Persson L (2001) Berggrundskarta 11I Uppsala NV, Sveriges Geologiska Undersökning, Af 210

Atekwana EA, Sauck WA, Werkema DD Jr (2000) Investigations of geoelectrical signatures at a hydrocarbon contaminated site. J Appl Geophys 44:167–180

Bowling JC, Harry DL, Rodriguez AB, Zheng C (2007) Integrated geophysical and geological investigation of a heterogeneous fluvial aquifer in Columbus Mississippi. J Appl Geophys 62:58–73

Bylund G (1973) Paleomagnetic study of Scanian Dolerites and Basalts. Geology Department, Lund University, Lund

Dahlin T (1997) Resistivitetsmätning för ingenjörs- och miljötilläpningar. Bygg & Teknik vol 4, pp 48–55

Dahlin T (2001) The development of DC resistivity imaging techniques. Comput Geosci 27:1019–1029

Dahlin T, Zhou B (2006) Multiple-gradient array measurements for multichannel 2D resistivity imaging. Near Surf Geophys 4:113–123

Dahlin T, Leroux V, Nissen J (2002) Measuring techniques in induced polarisation imaging. J Appl Geophys 50(3):279–298

Dahlin T, Wisén R, Zhang D (2007) 3D Effects on 2D resistivity imaging—modelling and field surveying results. 13th European meeting of environmental and engineering geophysics, 3–5 September, Istanbul, Turkey

Drahor MG, Göktürkler G, Berge MA, Özgür Kurtulmus T (2006) Application of electrical resistivity tomography technique for investigation of landslides: a case from Turkey. Environ Geol 50:147–155

Gharibi M, Bentley LR (2005) Resolution of 3-D electrical resistivity images from inversions of 2-D orthogonal lines. J Environ Eng Geophys 10:339–349

Klingspor I (1976) Radiometric age-determination of basalts, dolerites and related syenite in Skåne, southern Sweden. Geol För Stockh Förh 98:195–216

Leroux V, Dahlin T (2003) Site conditions requiring extra precautions for induced polarisation measurements. In: Proceedings of 9th meeting environmental and engineering geophysics, Prague, Czech Republic, 31 August–4 September 2003, O-052, p 4

Maia DFS, Castilho GP (2008) Assessing the cost-benefit of multicore cables and non-polarizable electrodes on shallow time-domain IP surveys. In: Proceedings of SAGEEP 2008

Möller H (1992) Beskrivning till jordartskartan Uppsala NV, Sveriges Geologiska Undersökning, Ae 113, p 92

Möller H (1993) Jordartskartan 11I Uppsala NV, Sveriges Geologiska Undersökning, Ae 113

Möller H, Stålhös G (1971) Beskrivning till jordartskartan Uppsala SV, Sveriges geologiska undersökning, Ae 9, p 69

Möller H, Stålhös G (1974) Beskrivning till jordartskartan Uppsala SO, Sveriges Geologiska Undersökning, Ae 10, p 80

Müllern C-F (1978) Den prekambriska berggrunden. I Gustafsson, O. Beskrivning till hydrogeologiska kartbladet Trelleborg NO/Malmö SO. SGU Ag 6, pp 8–13

Nichols TC Jr, Collins DS (1991) Rebound, relaxation, and uplift. In: Kiersch GA (ed) The heritage of engineering geology; the first hundred years. The Geological Society of America, pp 265–276

Palacky GJ (1989) Resistivity characteristics of geologic targets. In: Nabighian MN (ed) Electromagnetic methods in applied geophysics. Society of Exploration Geophysicist, pp 53–130

Papadopoulos NG, Tsourlos P, Tsokas GN, Sarris A (2007) Efficient ERT measuring and inversion strategies for 3D imaging of buried antiquities. Near Surf Geophys 5(6):349–361

Persson L (1988) Beskrivning till berggrundskarta Vetlanda SV, Sveriges Geologiska Undersökning, Af 170

Persson L (1989) Berggrundskarta 6F Vetlanda SV, Sveriges Geologiska Undersökning, Af 170

Räisänen M, Torppa A (2005) Quality assessment of a geologically heterogeneous rock quarry in Pirkanmaa county, southern Finland. Bull Eng Geol Environ 64:409–418

Ringberg B (1979) Jordartskartan 2C Malmö SO, Sveriges Geologiska Undersökning, Ae 38

Ringberg B (1980) Beskrivning till Jordartskartan Malmö SO, Sveriges Geologiska Undersökning, Ae 38, p 179

Sass O (2007) Bedrock detection and talus thickness assessment in the European Alps using geophysical methods. J Appl Geophys 62:254–269

Sivhed U, Erlström M (1998) Berggrundskartan 2C Malmö SO, Sveriges Geologiska Undersökning, Af 194

Slater LD, Lesmes D (2002) IP interpretation in environmental investigations. Geophysics 67:77–88

Telford WM, Geldart LP, Sheriff RE (1990) Applied geophysics, 2nd edn. Cambridge University Press, Cambridge, p 770

Wisén R, Linders F, Dahlin T (2006) 2D and 3D resistivity imaging in an investigation of boulder occurrence and soil depth in glacial till. 12th European meeting of environmental and engineering geophysics, 4–6 September, Helsinki, Finland

Zhou B, Dahlin T (2003) Properties and effects of measurement errors on 2D resistivity imaging surveying. Near Surf Geophys 1(3):105–117

Zonge K, Wynn J, Urquhart S (2005) Resistivity, induced polarization, and complex resistivity. In: Butler DK (ed) Near-surface geophysics. Society of Exploration Geophysicist, Tulsa, pp 265–300